Observation of a high grade of polarization of solitons generated in the process of pulse breakup in a twisted fiber

Ariel Flores-Rosas,[1] Josue I. Peralta-Hernandez,[2] Yazmin E. Bracamontes-Rodríguez,[3] Balder A. Villagomez-Bernabe,[2] Georgina Beltrán-Pérez,[3] Olivier Pottiez,[4] Baldemar Ibarra-Escamilla,[2] Roberto Rojas-Laguna,[1] and Evgeny A. Kuzin[2,*]

[1]*Division de Ingenerias, Campus Irapuato Salamanca, Universidad de Guanajuato, Carretera Salamanca-Valle de Santiago km 3.5+1.8 A.P. 215_A, Salamanca Gto., Mexico*
[2]*INAOE, Enrique Erro 1, Tonantzintla A.P. 72000 Puebla, Mexico*
[3]*Facultad de Ciencias Fisico Matematicas, Av. San Claudio y Rio Verde, San Manuel, Puebla, Mexico*
[4]*Centro de Investigaciones en Óptica, Loma del Bosque 115, Col. Lomas del Campestre, 37150 León, Gto., Mexico*
**Corresponding author: ekuz@inaoep.mx*

Received October 24, 2013; revised February 14, 2014; accepted February 19, 2014;
posted February 20, 2014 (Doc. ID 200138); published March 18, 2014

Common optical fibers are randomly birefringent, which results in random polarization of the supercontinuum (SC) generated in such fibers. Random polarization is undesirable for many applications of the SC. The formation of solitons from a pump pulse is one of the principal mechanisms of SC generation. Fiber twisting mitigates the random linear birefringence, which makes twisted fiber attractive for nonlinear applications. In this work we measured the polarization of solitons formed by the pulse breakup process. We found that a circularly polarized 1 ns pump pulse introduced to a twisted Corning SMF-28 fiber produces solitons with a high grade of circular polarization, while in a fiber without twist the polarization of solitons is random.

OCIS codes: (060.4370) Nonlinear optics, fibers; (060.5530) Pulse propagation and temporal solitons.
http://dx.doi.org/10.1364/JOSAB.31.000821

1. INTRODUCTION

Supercontinuum (SC) generation was observed when pumping by femtosecond [1–4], picosecond [5,6], and nanosecond [7–9] pulses as well as with continuous-wave (cw) light [10–12]. The nonlinear effects participating in SC generation include self-phase modulation, four-wave mixing, high-order soliton fission, modulation instability (MI), and stimulated Raman scattering (SRS) [13]. The interplay between nonlinear effects depends substantially on the pulse duration and the fiber length. An important role in SC formation is played by the pulse breakup process, resulting in soliton formation and subsequent soliton self-frequency shift (SSFS). Pulse breakup was observed in conventional fibers [14,15] and also in photonic crystal fibers (PCFs) [16]. When pumping by relatively long (>10 ps) pulses, MI, formation of solitons, and SSFS are dominant at the initial stage of the process. The process of MI starts from the noise affecting the pump pulses, and therefore the SC presents phase and amplitude fluctuations that lead to the degradation of the coherence of the SC and also may lead to the degradation of its polarization if the fiber length is longer than the beat length. The degradation of coherence was studied numerically and experimentally [17–20]. It was found that the degradation of coherence depends strongly on the duration and wavelength of the input pulse. In particular, shorter pulses were found to be less sensitive to noise than longer pulses. A comparison of experimental results with numerical simulations showed that the observed coherence degradation is consistent with fluctuations in the injected peak power significantly higher than the quantum limit.

Polarization properties of SC also are an important issue for applications [21–25]. The continuum generated is generally unpolarized, whereas many applications require a polarized SC. A natural reason for polarization degradation is the random residual birefringence that is always present in non-polarization-preserving fibers. Efforts were made to generate polarized SCs in high-birefringence fibers [21,22]. However a numerical analysis of the polarization of an SC generated in a weakly birefringent PCF undertaken in [23] shows that the noise imposed on the pump pulse also leads to polarization degradation. In the presence of noise, random polarization was found even if the input pulse was polarized precisely along one of the principal axes. The appearance of an orthogonal polarization component was explained as a result of the noise amplified by the vector MI. Experimental investigation of the polarization properties of SCs confirmed the previous numerical predictions about the SC polarization properties [24]. The analysis of the polarization properties requires solving the coupled generalized nonlinear Schrödinger equations. However, only a few papers analyzed SC generation using these coupled equations [23–25].

The twist of the fiber induces circular birefringence and also mitigates the residual linear birefringence, and both effects may affect the formation of solitons in the pulse breakup process. The twisted fiber is attractive for nonlinear applications, because unlike a standard nonpolarization-maintaining

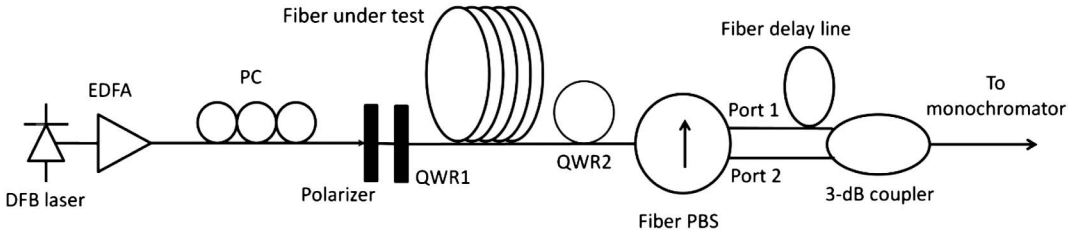

Fig. 1. Experimental setup.

fiber, where the polarization dependence of nonlinearity is averaged out by the residual birefringence, the twisted fiber behaves as a perfectly isotropic fiber [26]. The circular birefringence induced by twist moves the polarization of a single soliton to circular polarization during the propagation of the soliton [27].

In this paper we investigate the polarization of solitons formed as a result pumping by nanosecond-long pulses in a standard twisted fiber. We pump the fiber by 1 ns pulses at 1549.5 nm and measure the average polarization of the resulting bunch of solitons centered at 1560, 1570, and 1580 nm. When the twisted fiber is pumped by a circularly polarized input pulse, the solitons are mostly circularly polarized with about 90% of the power in the circularly polarized component, while the polarization of solitons formed in a fiber without twist is found to be random at any input polarization. Numerical investigations of the polarization of solitons show that the polarization is distributed randomly close to the polarization of the pump pulse; however, the average ellipticity is higher than the ellipticity of the pump pulse. The dispersion of the ellipticity gets smaller when the ellipticity of the pump is close to circular.

2. EXPERIMENTAL SETUP

The experimental setup is presented in Fig. 1.

As a signal source we used a cw distributed feedback (DFB) semiconductor laser emitting at a wavelength of 1549.5 nm. The cw signal is gated and amplified by the Er-doped fiber amplifier (EDFA) to obtain pulses with about a 1 ns duration and maximum peak power of 150 W. The pulses from the amplifier output pass through a polarization controller (PC) and a polarizer to ensure a stable polarization state. Rotation of the quarter-waver retarder QWR1 allows us to change the polarization ellipticity before launching the pulses into the fiber. The fiber output is connected to QWR2, which is actually formed by three loops of the fiber bent with a diameter of 50 mm, and to a fiber polarization beam splitter (PBS). QWR2 converts the right- and left-circularly polarized components at the fiber output to orthogonally polarized linear components. The angle between the axis of QWR2 and the PBS was adjusted to be 45°. These elements convert the right- and left-circularly polarized components at the fiber output to orthogonally polarized linear components at the PBS outputs. The pulses at the PBS outputs are separated in time by a delay line connected to port 1, and then using a 50/50 coupler they are combined and launched to a monochromator. The pulses are then detected by a photodetector and monitored by an oscilloscope. The first pulse to be detected is that coming from port 2 of the PBS, whereas the second pulse comes from port 1 through the delay line. With this setup we are able to measure the amplitudes of the left- and right-circularly polarized components at any wavelength in one single shot. A typical oscilloscope trace of the detected pulses is presented in Fig. 2. The ellipticity is calculated using the equation

$$\rho = \tan^{-1}\left(\frac{\sqrt{P_+} - \sqrt{P_-}}{\sqrt{P_+} + \sqrt{P_-}}\right), \tag{1}$$

where P_+ and P_- are the pulse amplitudes at the monochromator output.

The technique has some ambiguity when the measured ellipticity is low. The input pulse with any polarization can be considered as a sum of two pulses, left-circularly polarized and right-circularly polarized. Our measurement technique separates the left- and right-circularly polarized components so that they appear at port 1 and port 2, respectively, of the PBS. The amplitude of the first pulse on the oscilloscope corresponds to the energy of all components with left-circular polarization; the amplitude of the second pulse corresponds to the energy of all right-circularly polarized pulses. So what we measure is the average ellipticity in the bunch of pulses. Hence, a bunch of linearly polarized pulses has the same 0 average ellipticity as a bunch of pulses whose ellipticity is uniformly distributed around 0.

When the pulse at the fiber output is circularly polarized, the amplitude of one of the pulses in the oscilloscope trace is equal to 0. However, the minimal measurable amplitude is restricted by the noise of the detector. We estimated the maximal signal/noise ratio as 30, which gives us a maximal measurable ellipticity of 35°. Hence, values of the ellipticity higher than 35° cannot be distinguished from circular ellipticity. However, at this ellipticity 97% of the power is in one circularly polarized component, and only 3% is in the orthogonal

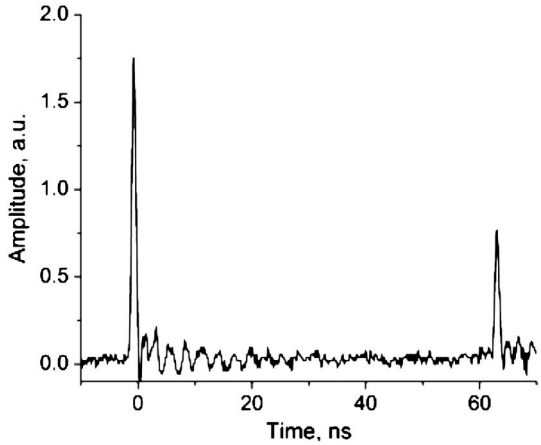

Fig. 2. Oscilloscope trace.

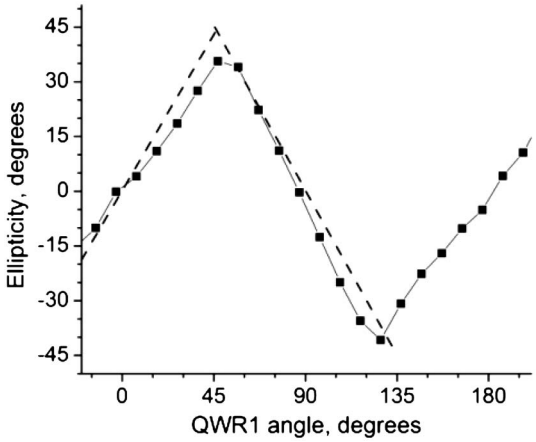

Fig. 3. Ellipticity at the QWR1 output measured by our setup (solid line); dashed line shows the ideal dependence of ellipticity on the QWR1 angle in the case of perfect measurements.

component. We calibrated our setup of ellipticity measurement by measuring the ellipticity directly at the QWR1 output. The result of this measurement is presented in Fig. 3. The angle 0 corresponds to the linearly polarized signal at the QWR1 output. Note that the ellipticity of the signal at the QWR1 output is equal to the angle of rotation of QWR1 in the range −45° to +45°.

As the fiber, we used several spans of SMF-28, either twisted or without twist.

As the next step, we measured the ellipticity at the fiber output at low power, when the nonlinear effects are not significant. As is well known, fiber twist induces circular birefringence and mitigates the residual linear birefringence. However, the linear birefringence of the fiber resulting from bending is not cancelled by twist, and the diameter of the cylinder on which the fiber is wrapped must be sufficiently large [26]. The measurements of the dependence of the output ellipticity on the input ellipticity show the effect of linear birefringence in the fiber. As an example, Fig. 4(a) shows the ellipticity at the output of a 218 m twisted fiber (5 turns/m) wrapped on a cylinder with a diameter of 25 cm; Fig. 4(b) shows the ellipticity at the output of a fiber of the same length and twist wrapped on a 50 cm cylinder. For the 25 cm diameter cylinder the effect of the linear birefringence can be clearly seen, as the curve deviates substantially from the ellipticity at the fiber input. However, for the 50 cm cylinder the ellipticity at the fiber output is close to the ellipticity at the fiber input. It means that there is no substantial effect of linear birefringence in the latter case. The fiber without twist shows dependence similar to that in Fig. 4(a). We used in our experiments a 218 m twisted fiber wrapped on a 50 cm cylinder and a fiber of the same length without twist.

3. RESULTS AND DISCUSSION

When pulses with a power of 150 W were launched into the fiber, pulse breakup occurred and was followed by soliton formation and SSFS. A typical spectrum at the output of the fiber with twist is shown in Fig. 5. The strong peak at 1655 nm is due to SRS that has maximal amplification at 1660 nm for 1550 nm pumping.

Some small fraction of energy was measured for wavelengths shorter than the pump wavelength. The formation

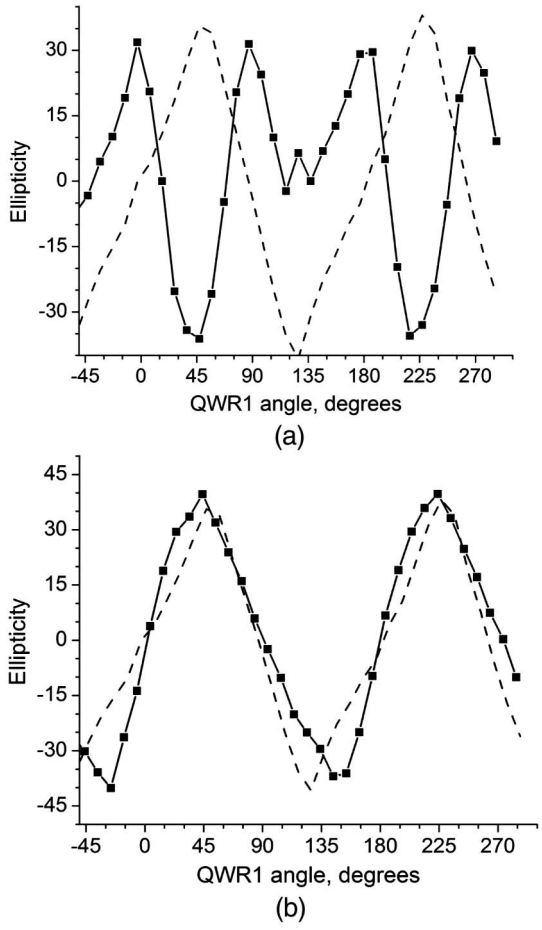

Fig. 4. Measured ellipticity at the output of the 218 m fiber (a) on a 25 cm spool and (b) on a 50 cm spool. The dashed line shows the input ellipticity.

of a broadband spectrum is a complex process involving several nonlinear effects. The different regimes of SC generation can be distinguished by considering short (femtosecond) versus long (picosecond, nanosecond, and continuous wave) pump pulses. The "long pulse" regime typically is considered for long high-power pump pulses for which the soliton number $N \gg 10$ [13]. The pulses considered here both in experiments and simulations can be considered as long pulses. In this case the effect of spontaneous MI dominates the initial stage of the

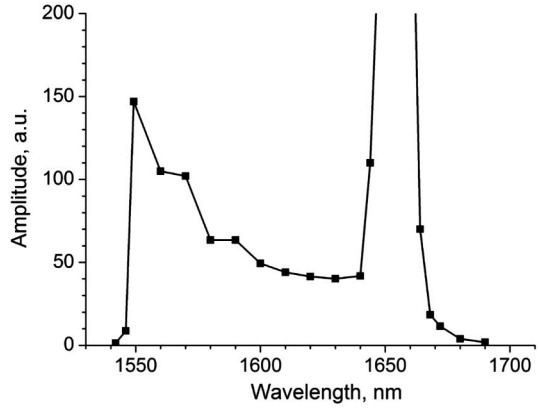

Fig. 5. Spectrum at the fiber output.

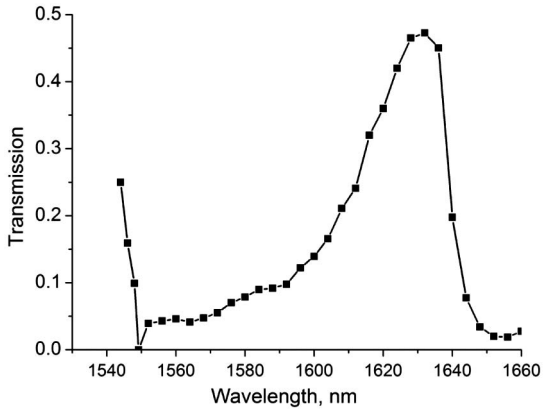

Fig. 6. Transmission through the NOLM.

broadband spectrum formation. MI results in pulse breakup and formation of short pulses that evolve finally to a bunch of solitons and dispersive waves. The solitons are shifted to longer wavelengths by SSFS. The solitons with higher power have a larger wavelength shift. The rate of spectrum shift is inversely proportional to the fourth power of the soliton duration or proportional to the square of the soliton power. So the measurement of the pulse power against the wavelength shift can give some additional useful information. Some insight into the peak power of the pulses can be obtained by measuring the transmission through a nonlinear optical loop mirror (NOLM). The transmission through the NOLM depends on the pulse power, which allows the estimation of the soliton power. We used a NOLM with a 50/50 coupler in which the nonlinear dependence of the transmission is achieved by polarization asymmetry [28]. We used an SMF-28 fiber of 5 m length in the loop. The critical power of the NOLM was calculated to be 2.4 kW. The transmission through the NOLM for a 150 W pump pulse can be calculated to be of the order of 10^{-2}. The transmission through the NOLM for the broadband light at the fiber output is shown in Fig. 6. We see very low transmission at the wavelength of the pump. The transmission grows with the wavelength and reaches about 50% at 1630 nm; this shows that pulses shifted to longer wavelengths have a higher peak power, which corroborates the SSFS mechanism. The measurement of the NOLM transmission allows the assumption that the spectrum between approximately 1560 and 1630 nm is formed substantially by soliton-like pulses. In contrast, the transmission through the NOLM for the Raman peak is low and indicates that this part of the spectrum has a different nature.

Figures 7–9 present the results of the measurements of the ellipticity at the fiber output. Input polarization is linear at QWR angles of 0°, 90°, etc.; polarization is circular at −45°, 45°, etc. For 1560 nm the average ellipticity at the output of the twisted fiber usually is close to the input ellipticity, except for some flattening of the dependence when the input ellipticity is close to circular, for QWR1 angles of 45°, 135°, and 225°. It can be seen that the radiation at the output of the twisted fiber presents a high grade of polarization, at least when the input polarization is circular. For an angle of QWR1 around 45°, about 90% of the output power is in the same circularly polarized component as the input pulse and only 10% is in the orthogonal component. For 1570 and 1580 nm the flatness of the dependence when input polarization is close to

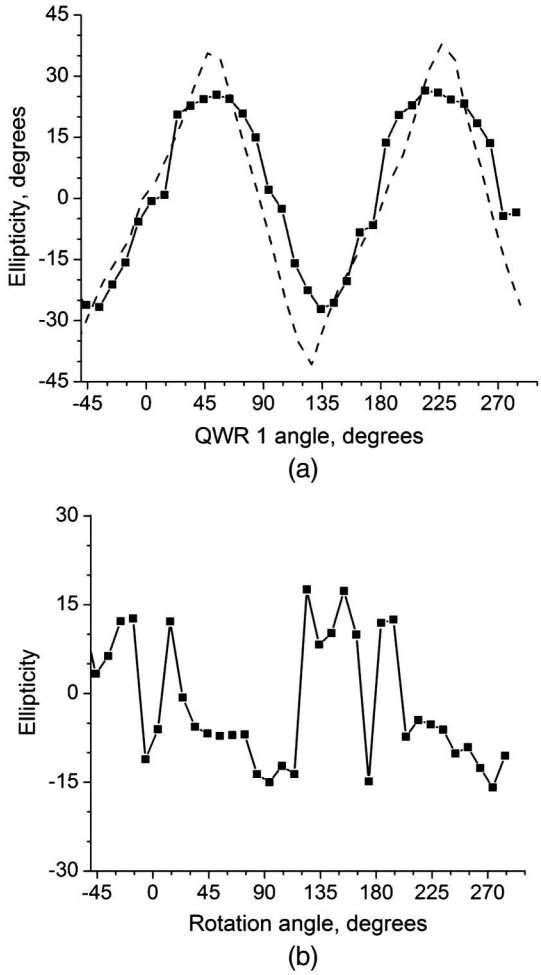

Fig. 7. Ellipticity at 1560 nm for (a) twisted fiber and (b) fiber without twist. The dashed line shows the input ellipticity.

circular can be clearly seen. In Fig. 9(a) the output ellipticity remains about 22° over a wide range of the QWR1 angle from 4° to 74°. After this the output ellipticity drops abruptly to −17°. The module of the slope of the output versus input ellipticity at input ellipticity equal to 0° was estimated to be 2 for 1570 and 1580 nm. For 1560 nm the module of the slope was estimated to be about 1. The module of the slope of the input ellipticity on the QWR1 angle is equal to 1. From these data it can be seen that the output ellipticity moves toward circularity faster than the input ellipticity over some range of input ellipticity close to 0°. For the fiber without twist both pulses on the oscilloscope trace were approximately equal at any input polarization. In this case Eq. (1) gives an ellipticity equal to 0. However, as was mentioned above, this just means that the energies of the left- and the right-circularly polarized components are equal. This value may correspond to linearly polarized pulses or to randomly polarized pulses. There are no physical reasons, however, to get linear output polarization for any input polarization, so we can assume that the polarization ellipticity of solitons is random at the output of the fiber without twist for any input polarization. An additional proof of the random polarization of the pulses is provided by the fact that the ratio of the amplitude of the pulses in the oscilloscope trace does not depend on the angle between the fiber PBS and QWR2. For linearly polarized pulses this dependence has to be clearly seen.

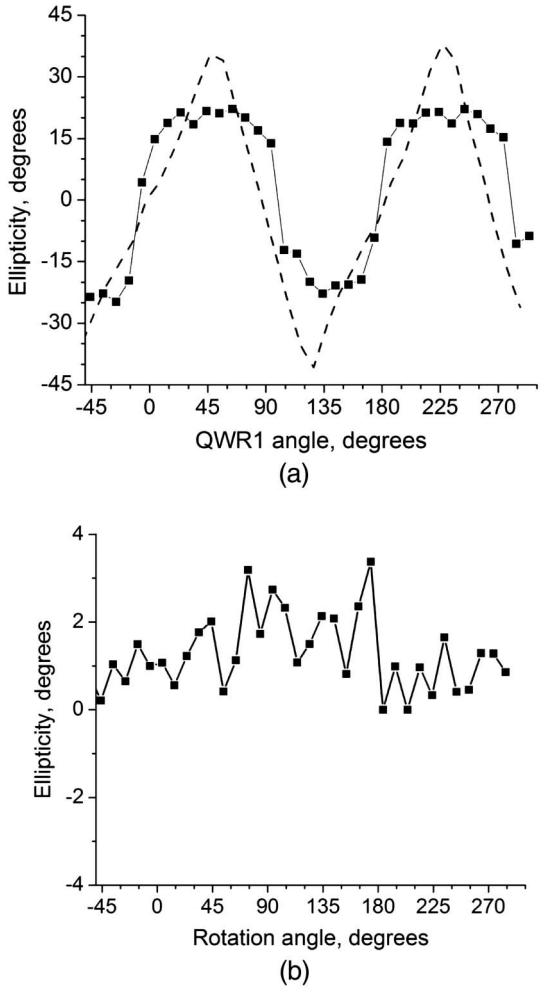

Fig. 8. Ellipticity at 1570 nm for (a) twisted fiber and (b) fiber without twist. The dashed line shows the input ellipticity.

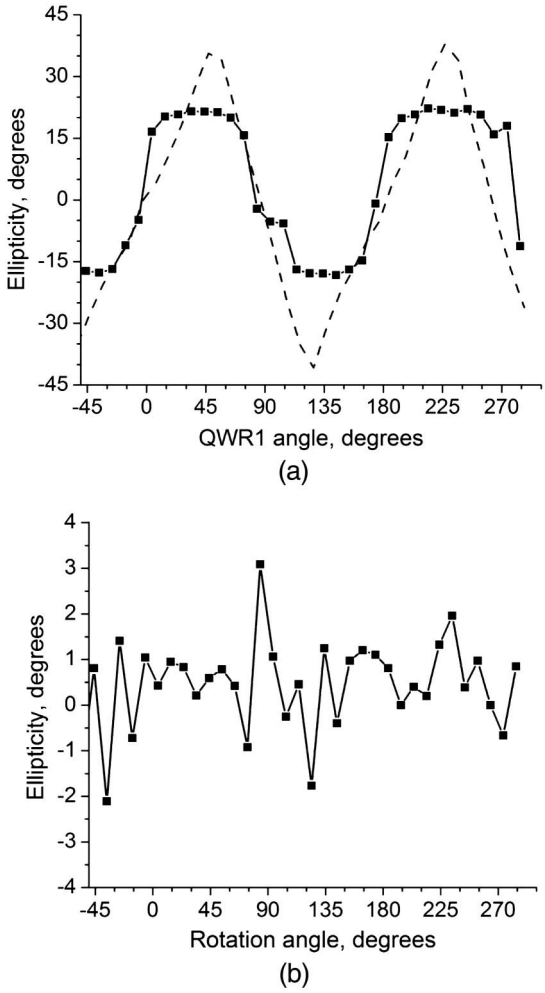

Fig. 9. Ellipticity at 1580 nm for (a) twisted fiber and (b) fiber without twist. The dashed line shows input ellipticity.

To support the observation that the solitons may have an ellipticity larger than the ellipticity of the pump, we calculated numerically the ellipticity of the solitons generated in the process of pulse breakup for different noises imposed on the pulse. For this simulation we used the equations and procedure described in [27]. The equations take into account the difference in group velocity between orthogonal circularly polarized components and the vectorial nature of the Raman effect in the fiber. We used as a pump a 30 ps pulse with 40 W of peak power. After a distance of approximately 1 km the pulse breakup results in the generation of a bunch of pulses. The pulse with the highest amplitude was selected from the bunch and represents the vector soliton we focus on. We investigated its ellipticity. Figure 10 shows the distribution of the output ellipticity for 50 shots. For this calculation we used $\beta_1 = 0.2$ ps/km and $\beta_2 = 25$ ps^2/km, where β_1 shows the delay between right- and left-circularly polarized components in the twisted fiber. The value 0.2 ps/km corresponds to 5 turns/m; β_2 is the group velocity dispersion, with the value corresponding to that of standard fibers. Input polarizations were equal to 0.4 (21.8°, black histograms in Fig. 9) and 0.9 (42°, white histograms). As we can see, in most shots the ellipticity of the soliton was higher than the ellipticity of the input pulse. For an input ellipticity equal to 0.4, the average output ellipticity is equal to 0.54; for an input ellipticity of 0.9, the average output ellipticity is equal to 0.95.

The calculations were done for different input polarizations. The dependence of the average soliton ellipticity on the input ellipticity is shown in Fig. 11. The calculations show some tendency for solitons to be generated with a higher

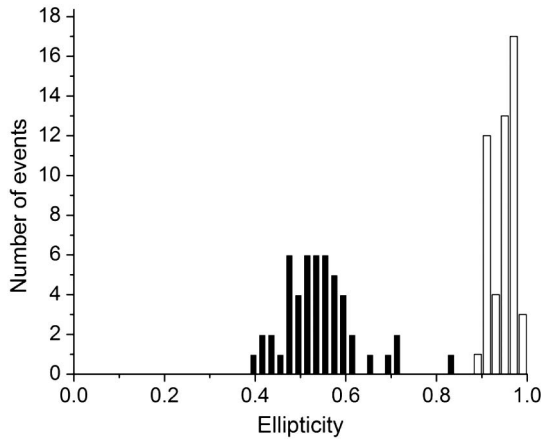

Fig. 10. Statistics of the ellipticity of the solitons with the highest amplitude.

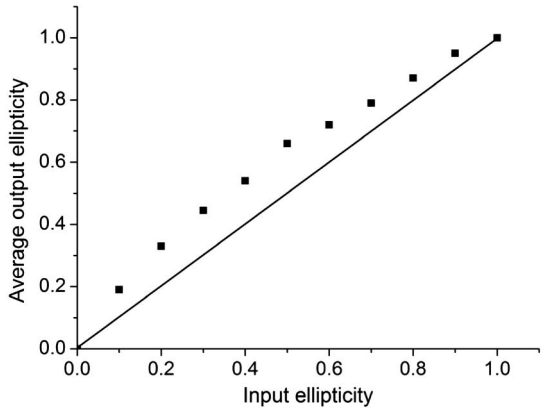

Fig. 11. Average output ellipticity versus input ellipticity; the squares show the results of the calculation, and the solid line indicates output ellipticity equal to input ellipticity.

ellipticity than the input pump pulse, as was observed in the experiments. It has to be noted, however, that the experimental conditions were not exactly the same as those used for the calculations, and for a more detailed comparison with the experimental data, much more extensive numerical work is required.

In conclusion, we showed that solitons generated in the process of pulse breakup in a twisted fiber have a high grade of polarization if the polarization of the input pulse is circular, while for solitons generated in the same fiber without twist, the polarization is random. Numerical calculations show that the polarization ellipticity of the solitons at the fiber output tends to be higher than the polarization of the input pulse. Experimental results show this tendency at input polarizations close to linear.

ACKNOWLEDGMENTS

The work was supported by CONACYT project 130966.

REFERENCES

1. G. A. Nowak, J. Kim, and M. N. Islam, "Stable supercontinuum generation in short lengths of conventional dispersion-shifted fiber," Appl. Opt. **38**, 7364–7369 (1999).
2. G. Genty, M. Lehtonen, H. Ludvigsen, J. Broeng, and M. Kaivola, "Spectral broadening of femtosecond pulses into continuum radiation in microstructured fibers," Opt. Express **10**, 1083–1098 (2002).
3. K. M. Hilligsøe, H. N. Paulsen, J. Thøgersen, S. R. Keiding, and J. J. Larsen, "Initial steps of supercontinuum generation in photonic crystal fibers," J. Opt. Soc. Am. B **20**, 1887–1893 (2003).
4. T. Hori, N. Nishizawa, T. Goto, and M. Yoshida, "Experimental and numerical analysis of widely broadened supercontinuum generation in highly nonlinear dispersion-shifted fiber with a femtosecond pulse," J. Opt. Soc. Am. B **21**, 1969–1980 (2004).
5. S. Coen, A. H. L. Chau, R. Leonhardt, J. D. Harvey, J. C. Knight, W. J. Wadsworth, and P. St. J. Russell, "White-light supercontinuum generation with 60 ps pump pulses in a photonic crystal fiber," Opt. Lett. **26**, 1356–1358 (2001).
6. S. Coen, A. H. L. Chau, R. Leonhardt, J. D. Harvey, J. C. Knight, W. J. Wadsworth, and P. St. J. Russell, "Supercontinuum generation by stimulated Raman scattering and parametric four-wave mixing in photonic crystal fibers," J. Opt. Soc. Am. B **19**, 753–764 (2002).
7. L. Provino, J. M. Dudley, H. Maillotte, N. Grossard, R. S. Windeler, and B. J. Eggleton, "Compact broadband continuum source based on a microchip laser pumped microstructured fiber," Electron. Lett. **37**, 558–560 (2001).
8. J. M. Dudley, L. Provino, N. Grossard, H. Maillotte, R. S. Windeler, B. J. Eggleton, and S. Coen, "Supercontinuum generation in air–silica microstructured fibers with nanosecond and femtosecond pulse pumping," J. Opt. Soc. Am. B **19**, 765–771 (2002).
9. P. A. Champert, S. V. Popov, and J. R. Taylor, "Generation of multiwatt, broadband continua in holey fibers," Opt. Lett. **27**, 122–124 (2002).
10. A. V. Avdokhin, S. V. Popov, and J. R. Taylor, "Continuous-wave, high-power, Raman continuum generation in holey fibers," Opt. Lett. **28**, 1353–1355 (2003).
11. A. K. Abeeluck, C. Headley, and C. G. Jørgensen, "High-power supercontinuum generation in highly nonlinear, dispersion-shifted fibers by use of a continuous-wave Raman fiber laser," Opt. Lett. **29**, 2163–2165 (2004).
12. A. K. Abeeluck and C. Headley, "Continuous-wave pumping in the anomalous- and normal-dispersion regimes of nonlinear fibers for supercontinuum generation," Opt. Lett. **30**, 61–63 (2005).
13. J. M. Dudley, G. Genty, and S. Coen, "Supercontinuum generation in photonic crystal fiber," Rev. Mod. Phys. **78**, 1135–1184 (2006).
14. P. Beaud, W. Hodel, B. Zysset, and H. P. Weber, "Ultrashort pulse propagation, pulse breakup, and fundamental soliton formation in a single-mode optical fiber," IEEE J. Quantum Electron. **23**, 1938–1946 (1987).
15. M. N. Islam, G. Sucha, I. Bar-Joseph, M. Wegener, J. P. Gordon, and D. S. Chemla, "Femtosecond distributed soliton spectrum in fibers," J. Opt. Soc. Am. B **6**, 1149–1158 (1989).
16. A. Ortigosa-Blanch, J. C. Knight, and P. St. J. Russell, "Pulse breaking and supercontinuum generation with 200-fs pump pulses in photonic crystal fibers," J. Opt. Soc. Am. B **19**, 2567–2572 (2002).
17. M. Nakazawa, K. Tamura, H. Kubota, and E. Yoshida, "Coherence degradation in the process of supercontinuum generation in an optical fiber," Opt. Fiber Technol. **4**, 215–223 (1998).
18. J. M. Dudley and S. Coen, "Coherence properties of supercontinuum spectra generated in photonic crystal and tapered optical fibers," Opt. Lett. **27**, 1180–1182 (2002).
19. J. M. Dudley and S. Coen, "Numerical simulations and coherence properties of supercontinuum generation in photonic crystal and tapered optical fibers," IEEE J. Quantum Electron. **8**, 651–659 (2002).
20. X. Gu, M. Kimmel, A. P. Shreenath, R. Trebino, J. M. Dudley, S. Coen, and R. S. Windeler, "Experimental studies of the coherence of microstructure-fiber supercontinuum," Opt. Express **11**, 2697–2703 (2003).
21. M. Lehtonen, G. Genty, H. Ludvigsen, and M. Kaivola, "Supercontinuum generation in a highly birefringent microstructured fibre," Appl. Phys. Lett. **82**, 2197–2199 (2003).
22. C. Xiong and W. J. Wadsworth, "Polarized supercontinuum in birefringent photonic crystal fiber pumped at 1064 nm and application to tunable visible/UV generation," Opt. Express **16**, 2438–2445 (2008).
23. Z. Zhu and T. G. Brown, "Polarization properties of supercontinuum spectra generated in birefringent photonic crystal fibers," J. Opt. Soc. Am. B **21**, 249–257 (2004).
24. Z. Zhu and T. G. Brown, "Experimental studies of polarization properties of supercontinua generated in a birefringent photonic crystal fiber," Opt. Express **12**, 791–796 (2004).
25. H. Tu, Y. Liu, X. Liu, D. Turchinovich, J. Lægsgaard, and S. A. Boppart, "Nonlinear polarization dynamics in a weakly birefringent all-normal dispersion photonic crystal fiber: toward a practical coherent fiber supercontinuum laser," Opt. Express **20**, 1113–1128 (2012).
26. T. Tanemura and K. Kikuchi, "Circular-birefringence fiber for nonlinear optical signal processing," J. Lightwave Technol. **24**, 4108–4119 (2006).
27. N. Korneev, E. A. Kuzin, B. A. Villagomez-Bernabe, O. Pottiez, B. Ibarra-Escamilla, A. González-García, and M. Durán-Sánchez, "Raman-induced polarization stabilization of vector solitons in circularly birefringent fibers," Opt. Express **20**, 24288–24294 (2012).
28. E. A. Kuzin, N. Korneev, J. W. Haus, and B. Ibarra-Escamilla, "Theory of nonlinear loop mirrors with twisted low-birefringence fiber," J. Opt. Soc. Am. B **18**, 919–925 (2001).